Journal of Materials Chemistry A

Accepted Manuscript

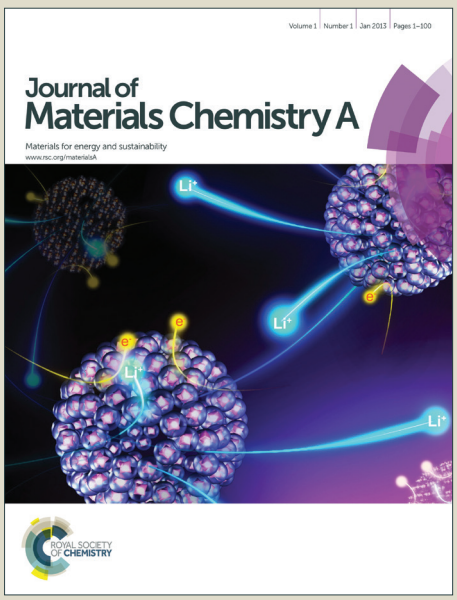

ROYAL SOCIETY OF CHEMISTRY

www.rsc.org/materialsA

Cite this: DOI: 10.1039/c0xx00000x

www.rsc.org/xxxxxx

ARTICLE TYPE

Engineering 2D Multi-Layer Graphene-like Co_3O_4 Thin Sheets with Vertically Aligned Nanosheet as Basic Building Units for Advanced Pseudocapacitor Materials

Liying Xuan[a], Lingyun Chen*[a], Qingqing Yang[a], Weifan Chen[b], Xiaohuan Hou[a], Yuqian Jiang[a], Qing Zhang[a] and Yuan Yuan[a]

Received (in XXX, XXX) Xth XXXXXXXXX 20XX, Accepted Xth XXXXXXXXX 20XX
DOI: 10.1039/b000000x

Olivaceous two-dimensional (2D) multi-layer graphene-like Co_3O_4 thin sheets (CQU-Chen-Co-O-1) with vertically aligned nanosheet as basic building units were first prepared on a large scale by direct hydrothermal decomposition of the mixed aqueous solution of cobalt (II) nitrate and acetic acid *without the assistance of any template or surfactant*. The resulting products exhibited excellent pseudocapacitive performance with high specific capacitance of 1752 and 1862 $F \cdot g^{-1}$ at 5 $mV \cdot s^{-1}$ and 1 $A \cdot g^{-1}$, respectively, as well as good rate capability (63.64% capacitance surplus) and high cycling performance (99.5% surplus after 2000 cycles).

1. Introduction

With the expense of resource, energy depletion and environmental pollution, urgent attention has been focused on clean and green energy storage and conversion technology, especially clean and high efficient electrochemical energy storage devices.[1] Among which, supercapacitors (SCs), also known as electrochemical capacitors (ECs), have been regarded as a promising electrochemical energy device due to their high power density, fast charge and discharge capability, high specific capacitance, long cycle life and excellent cycling stability.[2] In general, major electrode materials reported for SCs are divided into three types including carbon mateials, metal oxides/hydroxides and conducting polymers.[3] Carbon-based materials utilize the capacitance from electrochemical double layer SCs (EDLCs) arising from the electrostatic adsorption of eletrolyte ions on the surface of active materials. In contract, metal oxides/hydroxides and conducting polymers store charge by pseudocapacitors (PCs) through faradaic process associated with surface or near-surface redox reaction. In general, PCs can provide higher capacitance values than EDLCs owing to fast redox reaction and the performance of PCs largely depends on the electrode materials.

Because of their unique structures, excellent properties and potential applications in adsorbent, separation, catalysis and energy storage, transition metal oxides with micro- and nano-structures have attracted a great deal of attention over the past decade.[4] Among various transition metal oxides available for SCs, Co_3O_4 is one type of attractive electrode materials for PCs due to its low cost, environmental compatibility and especially high theoretical specific capacitance, as well as well defined electrochemical redox activity.[5] Recent research results indicate that the specific capacitance of Co_3O_4 electrode is critically dependent on their surface structure and crystalline property for the pseudocapacitors store charge in the first few nanometers from the surface.[3,5] And many solid state and solution strategies have been explored to prepare various two-dimensional (2D) and 3D complex Co_3O_4 nano-architectures for PCs, where the building blocks are nanoparticles, nanowires or nanosheets with diameter tens and hundreds of nanometers. And fine controlling the nano-architectures of Co_3O_4 will combine the features of micro- and nanostructures, which will improve the interface contact efficiency between active sites and electrolytes, serve as reservoirs for electrolyte ions to facilitate electrons and ions transport, and provide spaces for volume expansion during the cycling process.[5,6] Recently, it was reported that 2D thin nanosheets with porous structure is favorable to efficient ion and electron transport, and can better accommodate the structure change in electrochemical reaction.[7] By two steps of ionothermal and annealing, mesoporous Co_3O_4 sheet is obtained, which displays a specific capacitance of 238.4 $F \cdot g^{-1}$ at 2 $A \cdot g^{-1}$.[8] Porous Co_3O_4 sheets which exhibit a maximum specific capacitance of 288 $F \cdot g^{-1}$ at 1 $A \cdot g^{-1}$ can be fabricated by an alternating voltage induced method.[9] Ultralayered Co_3O_4 structures with high porosity and specific capacitance of 548 $F \cdot g^{-1}$ at 8 $A \cdot g^{-1}$ have been synthesized by a facile homogeneous precipitation process under hydrothermal conditions.[10] More recently, sub-3 nm Co_3O_4 nanofilms with maximum specific capacitance of 1400 $F \cdot g^{-1}$ at 1 $A \cdot g^{-1}$ are prepared via a nonsurfactant and substrate-free hydrothermal method.[11] Up to date, the urgent demand is to develop high quality 2D Co_3O_4 thin sheets with nanostructures in high volumes by means of simple methods *without the assistance of any template or surfactant* to create PCs with high performance.

Herein, a simple route for 2D multi-layer graphene-like Co_3O_4 thin sheets (CQU-Chen-Co-O-1) with vertically

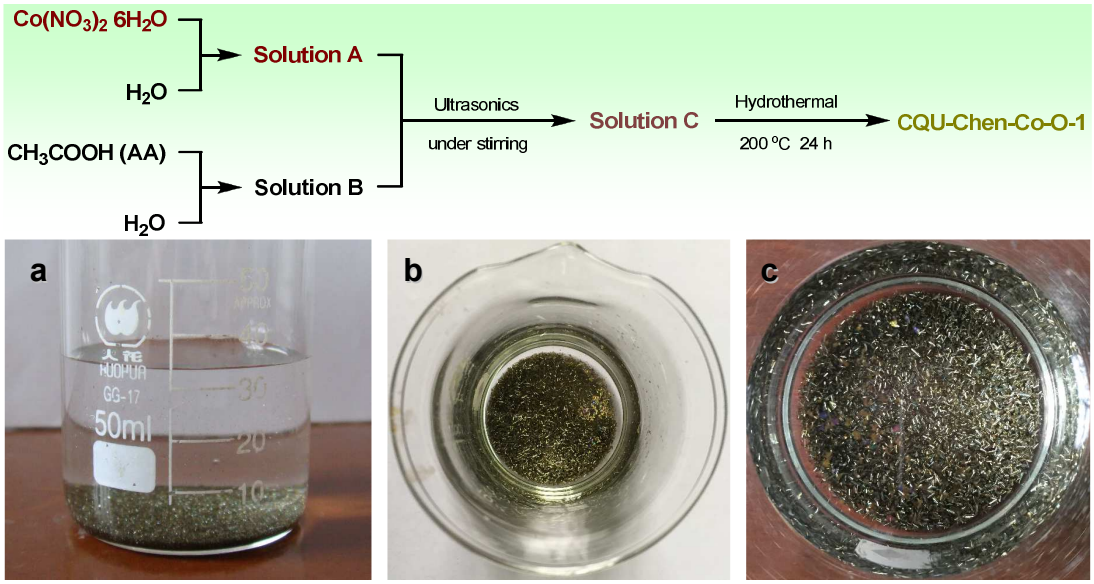

Fig. 1 Schematic illustration of the hydrothermal synthesis of the CQU-Chen-Co-O-1 from the mixed aqueous solution of cobalt (II) nitrate and AA and corresponding digital photography of the samples (a-c) in 50 ml beaker after hydrothermal reaction.

aligned nanosheet as basic building units was developed by direct hydrothermal decomposition of the mixed aqueous solution of cobalt (II) nitrate hexahydrate ($Co(NO_3)_2 \cdot 6H_2O$) and acetic acid (AA). The as-prepared products exhibit olivaceous sheet-like structures on a large scale in solution with digital photography in Fig. 1a-c. The CQU-Chen-Co-O-1 could be ideal candidates suitable for constructing energy storage devices with the advantages as follows: the 2D and 3D complex nano-architectures could make it easier to establish stable contacts for better electron transportation in the electrochemical electrodes and the high porosity of the materials composed by vertically aligned nanosheets generated on their surfaces may further offer efficient pathways for ion diffusion. The electrochemical properties of the materials are therefore evaluated by using them as building blocks to fabricate SCs.

The simple and facile hydrothermal process like our recent report for CQU-Chen-OA-Co-1-1[12] is schematically illustrated in Fig. 1. All the regents were purchased from Sinopharm Chemical Reagent Co. and used as received without further purification. $Co(NO_3)_2 \cdot 6H_2O$ as the source of cobalt, AA was used as the organic carboxylic acid, and Water as the solvent. In a typical procedure, 1 M $Co(NO_3)_2 \cdot 6H_2O$ and 2 M AA in water solvent are first mixed under ultrasonics and mechanical agitation for half an hour and then hydrothermally treated. All the reactions were performed in Teflon-lined stainless steel autoclaves (50 mL) with a filling rate of 60 %, which was maintained at 200 °C for 24 h and then cooled to room temperature naturally. Olivaceous products were collected by centrifuging and washed with water and absolute ethanol several times. Subsequently, these precipitates were frozen for 2 h followed by freeze-drying overnight. Impressively, the as-obtained CQU-Chen-Co-O-1 exhibited high specific capacitance and remarkable cycling stability as an electrode material for SCs.

2. Results and discussion

The crystal structure and phase purity of the CQU-Chen-Co-O-1 are investigated by X-ray powder diffraction (XRD) as shown in Fig. 2a. Almost all the diffraction peaks at (111), (220), (311), (222), (400), (422), (511), (440) and (531) of the product can be indexed to the standard Co_3O_4 crystal structure (sys: Cubic, lattice: Face-centered, cell parameters: a = 8.083 Å, JCPDS card no. 42-1467). As shown in Fig. 2b of the crystal structure, Co_3O_4 is a normal spine1 based on a cubic close-packing array of oxide ions where one-eighth of tetrahedral interstices are occupied by high-spin Co^{2+} ions, and one-half of octahedral interstices are occupied by low-spin Co^{3+} ions at room temperature.[13] Fig. 2c and S2 display the Raman spectra of the products. Three obvious peaks are located at 460, 506, and 658 cm^{-1}, which are correspond to $1E_g$, $F_{2g}{}^1$ and 1 A_{1g} Raman active modes of the Co_3O_4. The phonon symmetries of the Raman peaks are caused by the lattice vibrations of the spinal structure, in which Co^{2+} and Co^{3+} cations are situated at tetrahedral and octahedral sites in the cubic lattice.[14] In addition, the composition of the as-prepared CQU-Chen-Co-O-1 was investigated through the energy dispersive X-ray analysis (EDX) in Fig. 2d. Obviously, the element of Au came from the prinkled Au for SEM investigation of the sample, while the ratio of Co and O is identical with the composition of Co_3O_4. All the results indicate that pure Co_3O_4 has been successfully synthesized via a simple hydrothermal method.

The morphology and structure of the as-prepared CQU-Chen-Co-O-1 were investigated by field emission scanning electron microscopy (FE-SEM) and transmission electron microscopy (TEM) in Fig. 3. Fig. 3a-d show different magnification SEM images of the CQU-Chen-Co-O-1. As shown in Fig. 3a of low magnification SEM image, large-scale of sheet-like products were obtained with the width of

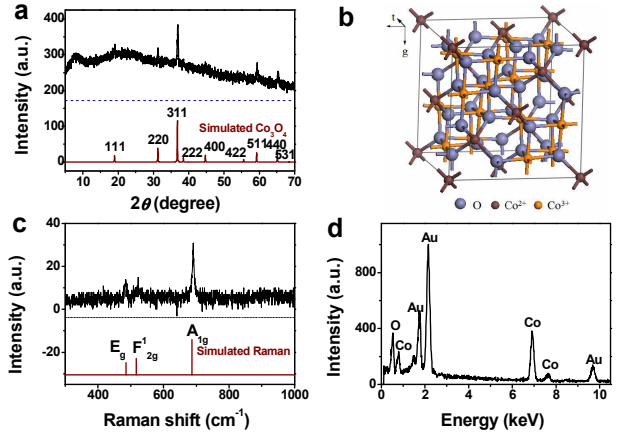

Fig. 2 (a) XRD patterns of the products and the simulated XRD patterns of Co_3O_4, (b) Crystal structure of spinel Co_3O_4, (c) Raman spectra and (d) EDX spectra of the products.

hundreds of micrometerials, which is consistent with the digital photography in Fig. 1. From high magnification SEM images in Fig. 3b-d, the as-prepared CQU-Chen-Co-O-1 exhibits sheet-like structures with vertically aligned nanosheet as basic building units and obvious porous structures with aperture of tens of nanometers composed by vertically aligned nanosheets with thickness of about 20 nm can be seen from SEM image in Fig. 3c and d. The porosity will provide efficient pathways for ion diffusion during the electrochemical testing process. Furthermore, TEM images in Fig 4a-c further indicate that the as-prepared CQU-Chen-Co-O-1 displays 2D fold-shaped and multi-layer graphene-like structures with width of hundreds of micrometerials and thickness of about 20 nm, which agrees with the SEM results. In addition, the corresponding selected-area electron diffraction (SAED) pattern of the CQU-Chen-Co-O-1 inset in Fig. 4c shows well-defined diffraction rings revealing the polycrystalline features of the cubic Co_3O_4 phase, which is consistent with the XRD patterns in Fig. 2a.

The electrochemical properties of the CQU-Chen-Co-O-1 as electrode materials for SCs were evaluated by cyclic voltammetry (CV), galvanostatic charge−discharge (GCD) measurement and electrochemical impedance spectroscopy (EIS) in 6.0 M KOH solution using a three electrode system at room temperature. Fig. 5a shows the CV curves at various scan rates ranging from 5 to 100 $mV \cdot s^{-1}$ in a potential range of 0.0 to 0.35 V versus SCE. The shapes of the present CV curves are distinctly different from the CV curves of EDLCs and a couple of redox peaks are visible in the CV curves, which shows oxidation (anodic) and reduction (cathodic) events of PCs. This indicates that the electrochemical capacitance of the Co_3O_4 electrode mainly results from the pseudocapacitance behavior caused by the following two faradic redox reactions[15]:

$$Co_3O_4 + OH^- + H_2O \rightarrow 3CoOOH + e^- \quad (1)$$

$$CoOOH + OH^- \rightarrow CoO_2 + H_2O + e^- \quad (2)$$

wherein, the potential difference between anodic and cathodic peaks increased due to the polarization of the electrode under a high scan rate. Additionally, the peak current increases with an increase in the scan rate, which suggests its good reversibility during the fast charge–discharge process. At a scan rate of 5 $mV \cdot s^{-1}$, the CV curve exhibits a shoulder peak at around 0.25 V, and a corresponding cathodic peak at about 0.16 V. As the scan rate increases, anodic peaks shift to higher potential and cathodic peaks shift to lower potential and the current density peaks increase with increasing scan rate which may caused by the limitation of the ion diffusion rate to satisfy electronic neutralization during the redox reaction. Moreover, as a result of insufficient faradic redox reaction at higher scan rate, the capacitance of Co_3O_4 decreases inevitably. The specific capacitance of the supercapacitor was calculated from the CV according to equation (3):

$$C_a = \frac{Q}{\Delta V} = \frac{1}{mv(V_1 - V_2)} \int_{V_2}^{V_1} I(V) dV \quad (3)$$

where C ($F \cdot g^{-1}$) is the specific capacitance of the electrode materials, m (g) is the mass of the electrode materials, v represents the scan rate, V_1 and V_2 refer to the high and low potential limit of the CV curves, $I(V)$ is the instant current on CV curves and $\triangle V$ is the potential window. Fig. 5b shows that there are linear relationships between the currents of both cathodic and anodic redox peaks and the square root of the scan rate, which indicates that the electrochemical process is a diffusion-controlled process of OH^- with rapid redox reactions of the CQU-Chen-Co-O-1. Furthermore, Fig. 5c demonstrates the specific capacitance of the CQU-Chen-Co-O-1 from the CV curves at different scan rates. At the scan rates of 5, 10, 20, 30, 50 and 100 $mV \cdot s^{-1}$, the corresponding specific capacitance is 1752, 1370, 1077, 949, 811 and 651 $F \cdot g^{-1}$, respectively. It was found that specific capacitance decreases with the increase of scan rate, suggesting the measured capacitance is mainly associated with the redox reaction. At a low scan rate, both the inner and outer surface of the material could be reached, whereas with the increase of the scan rate, the diffusion of the ions might more likely happen on the outer rather than inner surface of the nanostructure. Nevertheless, the not sharp decrease of the specific capacitance demonstrates that the porous and nanostructured products might act as a buffering reservoir to accommodate OH^- which in turn shortens the path of the ionic transport and relieves the fading of specific capacitance.

The GCD curves of the as-prepared CQU-Chen-Co-O-1 electrode at different current densities in the potential range from 0.0 to 0.35 V are shown in Fig. 5d. Among which, the two discharge flats of each curve are in accordance well with the two pairs of redox peaks in the CV curves, further confirming the pseudocapacitance property of the as-prepared products.The specific capacitance was also calculated from GCD curves according to equation (4):

$$C_s = I\Delta t / (m\Delta V) \quad (4)$$

where C ($F \cdot g^{-1}$) is the specific capacitance of the electrode materials, m (g) is the mass of the electrode materials, I is the current during the discharge process, $\triangle t$ (s) is the discharge time and $\triangle V$ is the potential window. From which, the corresponding specific capacitance is 1862, 1615, 1485, 1342 and 1185 $F \cdot g^{-1}$ at current densities of 1, 2, 3, 5, and 10 $A \cdot g^{-1}$, respectively, as plotted in Fig. 5e. And 63.64 % of the initial capacitance could be retained when the current density increased from 1 to 10 $A \cdot g^{-1}$, indicating the excellent rate

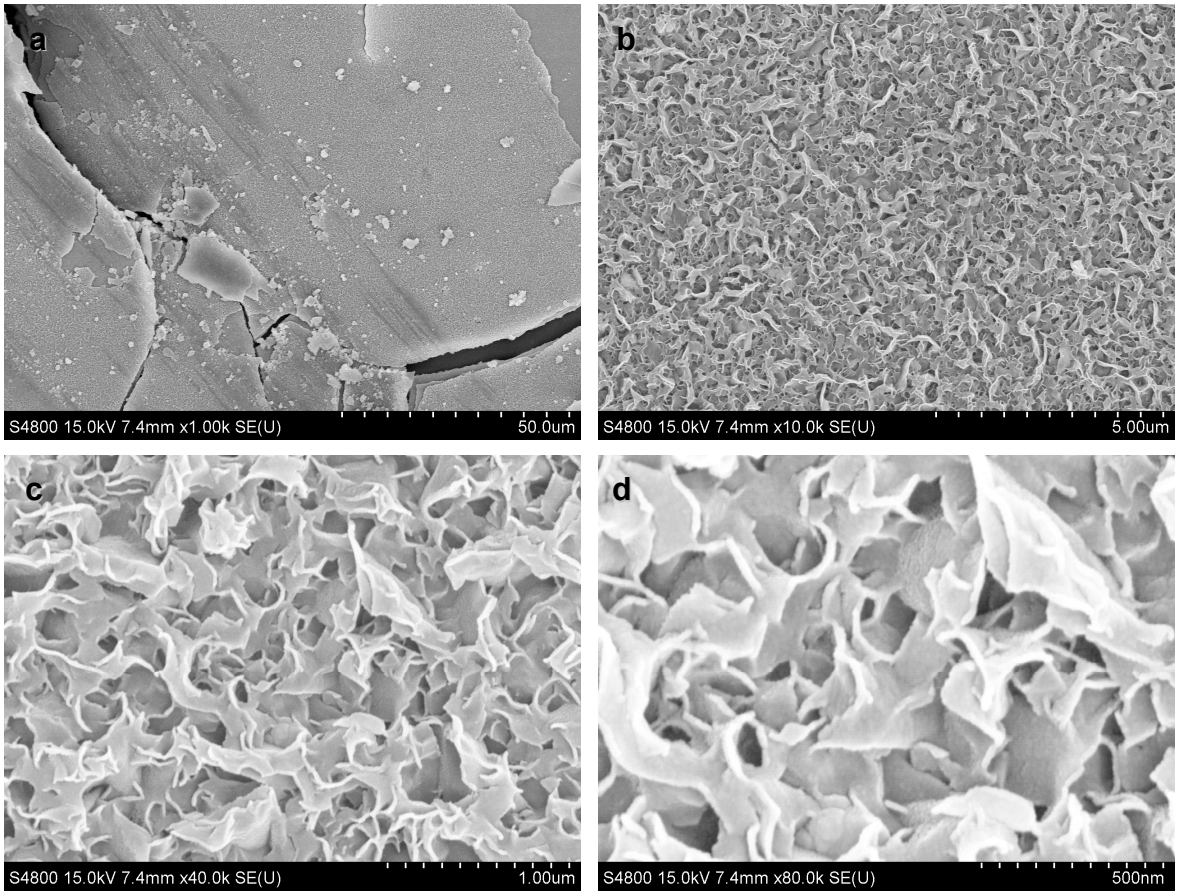

Fig. 3 (a)-(d) FE-SEM images of the as-prepared CQU-Chen-Co-O-1 at various magnifications.

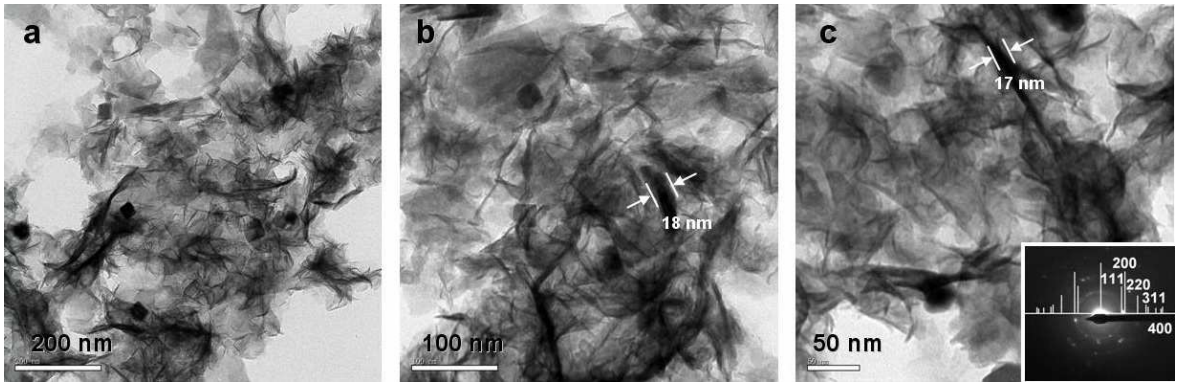

Fig. 4 (a)-(c) TEM images of the as-prepared CQU-Chen-Co-O-1 at various magnifications, inset of the corresponding SAED pattern.

capability of the as-prepared electrode.[16] In general, the boost of current density would result in fading in the capacitance value possibly owing to the internal resistance and polarization of the electrode. With increasing scan rate, the specific capacitance decreases gradually, which can be attributed to electrolytic ions diffusing and migrating into the active materials at low scan rates. At high scan rates, the diffusion effect, limiting the migration of the electrolytic ions, causes some active surface areas to become inaccessible for charge storage. This result indicates the excellent capacitive behavior and high-rate capability of the products.

As for SCs, the specific energy and power densities are the two important factors for the practical applications. The agone plot of the estimated specific energy and specific power of the as-prepared CQU-Chen-Co-O-1-base electrode is shown in Fig. 5f at various charge–discharge rates from Fig. 5d. The specific energy density (E) and power density (P) are calculated from the following equations of (5) and (6):

$$E = 1/2[C_s(\Delta V)^2] \quad (5)$$

$$P = E/\Delta t \quad (6)$$

where E ($Wh \cdot g^{-1}$) is the energy density, P ($W \cdot g^{-1}$) is the power density and ΔV is the operating of potential window, Δt (h) is the total discharge time. The excellent capability of delivering high specific power and energy densities indicates that the as-prepared thin sheets is suitable for SCs.[17]

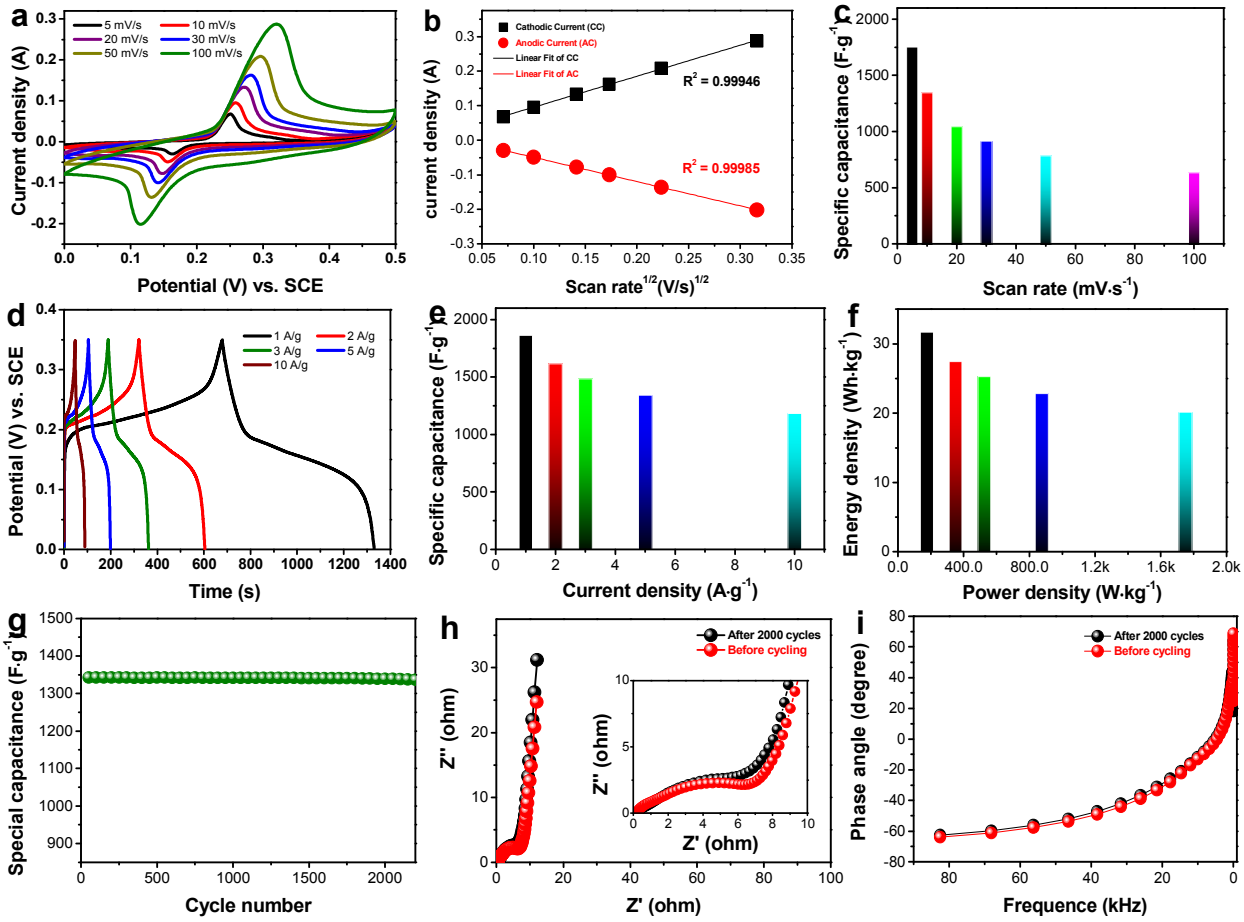

Fig. 5 Electrochemical performance of the CQU-Chen-Co-O-1-based electrodes: (a) CV curves at different scan rates of 5, 10, 20, 30, 50 and 100 mV·s^{-1}; (b) the variation of current densities of the cathodic and anodic peaks as a function of the square root of scan rate; (c) the correlation profiles of the scan rate and specific capacitance; (d) charge–discharge profiles at various current densities of 1, 2, 3, 5, 10 and 20 A·g^{-1}; (e) the correlation profiles of current density and specific capacitance; (f) Ragone plots of the estimated specific energy and specific power of the samples at various charge–discharge rates; (g) cycling performance at a constant current density of 5 A·g^{-1}; (h) Nyquist plots over the frequency range of 0.01 Hz to 100 kHz and (i) the phase angles for impedance plots before and after 2000 cycles at 5 A·g^{-1}.

The cycling performance of the CQU-Chen-Co-O-1-based electrode is evaluated under GCD measurement at a current densities of 5A·g^{-1} for 2000 cycles (in Fig. 5g). The specific capacitance of the as-prepared electrode keeps 95.5 % of its initial value after 2000 cycles, evidently indicating its superior cycling stability.

The electrochemical process is further investigated by electrochemical impedance spectroscopy (EIS) which was conducted to determine the electrode kinetics by applying an AC voltage with an amplitude of 5 mV in a frequency range from 0.01 Hz to 100 kHz, where Z' and Z'' are the real and imginary parts of the impedance, respectively. Fig. 5h shows the Nyquist plots of the CQU-Chen-Co-O-1 electrode before and after 2000 cycles. From which, both of the two Nyquist plots display a small semicircle in the high-frequency region and a straight linear part in the low-frequency region. Among which, the semicircle with the diameters representing the charge-transfer resistance (Rct) in the high frequency region is attributed to the three sections: electrolyte, electroactive material and the contact resistance between the electroactive material and the current collector, and the straight line is related to the diffusive resistance. In general, a smaller semicircle at high-frequency region means a minor charge–transfer resistance and the more vertical the line at low-frequency region, the more closely the supercapacitor behaves as an ideal capacitor.[18] Furthermore, the intercept of Z′ at very high frequencies represents equivalent series resistance (ESR) including the inherent resistance of the electroactive material, the bulk resistance of electrolyte, and the contact resistance at the active material/current collector interface.[19] Moreover, the intersection of the plot at the X-axis represents the solution resistance (Rs), which is composed of the KOH electrolyte resistance, the intrinsic resistance of the electroactive materials and the contact resistance between the active material and the current collector. Measured from the the magnifying EIS spectra inset in Fig. 5h, the calculated Rs and Rct values of the CQU-Chen-Co-O-1 electrode before and after 2000 cycles are 0.28 and 0.29 Ω as well as 5.7 and 5.9 Ω, respectivity. In addition, Fig. 5i shows the phase angles for impedance plots of the CQU-Chen-Co-O-1 electrodes before and after 2000 cycles. Both the two phase angles are near 70° in the low frequencies clearly, which reveals that the CQU-Chen-Co-O-1 allow ions or electrolyte transfer to occur.[20] All these results reveal that there is no obvious differences of the

Table 1 Comparison of various 2D and 3D Co_3O_4 nanostructures used as electrode materials for PCs synthesized via various methods without any supporting template.

Dimension	Nanostructures	Synthesis	Electrolyte	SC ($F \cdot g^{-1}$)	Current density	Cycling performance	Ref.
2D	Hexagonal sheets	Thermal decomposition	3 M KOH	92	5 $mA \cdot cm^{-2}$	93 % from 5 to 20 $mA \cdot cm^{-2}$	22
	Layered structures with rectangular flakes	Hydrothermal-calcination	6 M KOH	263	1 A g^{-1}	89.4 % over 1000 cycles at 3 $A \cdot g^{-1}$	23
	Mesoporous sheets	Ionothermal-calcination	2 M KOH	238.4	2 A g^{-1}	94.4 % over 4000 cycles at 2 $A \cdot g^{-1}$	8
	Porous sheets	Alternating voltage induced method	2 M KOH	288	1 A g^{-1}	79.0 % over 2000 cycles at 1 $A \cdot g^{-1}$	9
	Hexagonal platelets	Solvothermal	2 M KOH	476	0.5 A g^{-1}	82.0 % over 2000 cycles at 2.5 $A \cdot g^{-1}$	24
	Rectangular flakes	Precipitation-hydrothermal	1 M KOH	548	8 $A \cdot g^{-1}$	98.5 % over 2000 cycles at 16 $A \cdot g^{-1}$	10
	Sub-3 nm atomic layers nanofilms	Hydrothermal	2 M KOH	1400	1 A g^{-1}	97.1 % over 1500 cycles at 2$A \cdot g^{-1}$	11
3D	Oval-shaped microparticles	Hydrothermal-calcination	2 M KOH	111	2.5 $mA \cdot cm^{-2}$	88.2 % over1000 cycles at 2.5 $mA \cdot cm^{-2}$	25
	Mesoporous tubes	Biomorphic synthesis	OH^-	128.3	1 A g^{-1}	91.7 % over 3000 cycles at 1 $A \cdot g^{-1}$	26
	Porous structures	Solid-state thermolysis	2 M KOH	150	1 A g^{-1}	Recycling stability over 3400 cycles at 1 A g^{-1}	15
	Dendrite-like nanostructures	Calcination	3 M KOH	207.8	0.5 $A \cdot g^{-1}$	97.5 % over 1000 cycles at 1.8 $A \cdot g^{-1}$	27
	Tunable hierarchical morphologies	Calcination	6 M KOH	218	1.25 $A \cdot g^{-1}$	1000 cycles without degradation	28
	Multi-shelled hollow microspheres	Low-temperature Solution-aneal	2 M KOH	394.4	2 A g^{-1}	92 % over 500 cycles at 2 $A \cdot g^{-1}$	29
	Brush-like structures	Multistep hydrothermal	6 M KOH	407.5	1 $A \cdot g^{-1}$	97.5 % over 2000 cycles at 1 $A \cdot g^{-1}$	30
	Flower-like structures	Hydrothermal	3 M KOH	483.8	1 $A \cdot g^{-1}$	89.5 % over 2000 cycles at 10 $A \cdot g^{-1}$	31
	Hierarchical macro-mesoporous structures	Sol-gel	2 M KOH	742.3	0.5 $A \cdot g^{-1}$	87.2 %over 2000 cycles at 20 $mV \cdot s^{-1}$	32
	Urchin-like twin-spheres	Calcination	KOH	754	1 $A \cdot g^{-1}$	97.8 % over 1000 cycles at 4 $A \cdot g^{-1}$	33
	Enoki mushroom-like structures	Reflux	6 M KOH	787	1 $A \cdot g^{-1}$	94.5 % over 1000 cycles at 10 $A \cdot g^{-1}$	34
	Nanonet hollow structures	Calcination	6 M KOH	820	5 $mV \cdot s^{-1}$	90.2 % over 1000 cycles at 5 $A \cdot g^{-1}$	35
	Hierarchical structures	Precipitation-thermal treatment	6 M KOH	896	1 $A \cdot g^{-1}$	94.8 % over 5000 cycles at 10 $A \cdot g^{-1}$	36
	Hierarchical nanostructures	Calcination	6 M KOH	982	1 $A \cdot g^{-1}$	92.3 % over 1000 cycles at 4 $A \cdot g^{-1}$	37
	Nanonet-like structures	Solvothermal	6 M KOH	1063	10 $mA \cdot cm^{-2}$	90.8 % over 1000 cycles at10 $mA \cdot cm^{-2}$	38
	Porous hollow rhombic dodecahedral structures	Calcination	3 M KOH	1110	1.25 $A \cdot g^{-1}$	Almost no changes after 2000 cycles at 6.25 $A \cdot g^{-1}$	39
2D/3D	CQU-Chen-Co-O-1	Hydrothermal	6 M KOH	1752 and 1862	5 $mV \cdot s^{-1}$ and 1 $A \cdot g^{-1}$	99.5 % over 2000 cycles at 5 $A \cdot g^{-1}$	Our work

EIS spectra before and after 2000 cycles, which indicates that the CQU-Chen-Co-O-1 electrode is suitable for SCs.

Nanoscale design of the structure and chemistry of electrode materials may enable us to develop a new generation of devices that approach the theoretical limit for electrochemical storage and deliver electrical energy rapidly and efficiently.[21] Various 2D and 3D Co_3O_4 nanostructures synthesized *without using any supporting template* have been reported for the electrode materials of PCs listed in Table 1. Compared with the reported results, the CQU-Chen-Co-O-1-based electrode displays superior electrochemical performance attributed to its distinctive structures of 2D multi-layer graphene-like and porous thin sheets with vertically aligned nanosheet as basic building units, which fcilitates electron transportation and ion diffusion during the electrochemical testing process for PCs.

3. Conclusions

In summary, we have developed a simple route for 2D multi-layer graphene-like Co_3O_4 thin sheets (CQU-Chen-Co-O-1) via direct hydrothermal decomposition of the mixed aqueous solution of $Co(NO_3)_2$ and AA. The CQU-Chen-Co-O-1 with vertically aligned nanosheet as basic building unit

exhibits excellent electrochemical behaviors for PCs. In prospect, such a route will undoubtedly become an essential synthetic strategy in the design and synthesis of 2D multi-layer graphene-like metal oxide nanostructures and bring rapid development of new electrode materials with high performance for SCs.

Acknowledgements

We thank A. P. Xueqiang Qi for his help for Raman spectra measurements. This work is supported by the National Natural Science Foundation of China (Grant no. 21101176, 51464033 and 21061011), the Natural Science Foundation Project of CQ CSTC (no. 2010BB4232), the Fundamental Research Funds for the Central Universities (Project no. 106112015CDJXY228801, DXWL-2012-014, DXWL-2012-037 and CDJRC10220011, Chongqing University, China), and the Large-scale Equipment Sharing Fund of Chongqing University.

Notes and references

[a] *Chongqing Key Laboratory of Chemical Process for Clean Energy and Resource Utilization, School of Chemistry and Chemical Engineering, Chongqing University, Chongqing 400044, China. E-mail: lychen@cqu.edu.cn; chenlingyun@126.com*

[b] *School of Materials Science and Engineering, Nanchang University, Nanchang 330031, China*

† Electronic Supplementary Information (ESI) available: details of experimental and characterization as well as additional figures. See DOI: 10.1039/b000000x/

‡ Footnotes should appear here. These might include comments relevant to but not central to the matter under discussion, limited experimental and spectral data, and crystallographic data.

1 B. Dunn, H. Kamath and J. M. Tarascon, True Performance Metrics in Electrochemical Energy Storage, *Science*, 2011, **334**, 928–935.

2 B. E. Conway, *Electrochemical Supercapacitor Scientific Fundamentals and Technological Applications*, Springer, 1999.

3 P. Simon and Y. Gogotsi, Materials for Electrochemical Capacitors, *Nat. Mater.*, 2008, **7**, 845–854.

4 (a) J. Jiang, Y. Y. Li. J. P. Liu, X. T. Huang, C. Z. Yuan and X. W. Lou, Recent Advances in Metal Oxide-based Electrode Architecture Design for Electrochemical Energy Storage, *Adv. Mater.*, 2012, **24**, 5166–5180; (b) D. Che, Q. F. Wang, R. M. Wang and G. Z. Shen, Ternary Oxide Nanostructured Materials for Supercapacitors: A Review, *J. Mater. Chem. A*, 2015, **3**, 10158–10173.

5 (a) C. Z. Yuan, L. Yang, L .R. Hou, L. F. Shen, F. Zhang, D. K. Li and X. G. Zhang, Large-Scale Co_3O_4 Nanoparticles Growing on Nickel Sheets via a One-Step Strategy and Their Ultra-Highly Reversible Redox Reaction toward Supercapacitors, *J. Mater. Chem.*, 2011, **21**, 18183–18185; (b) C. Z. Yuan, L. Yang, L. R. Hou, J. Y. Li, Y. X. Sun, X. G. Zhang, L. F. Shen, X. J. Lu, S. L. Xiong and X. W. Lou, Flexible Hybrid Paper Made of Monolayer Co_3O_4 Microsphere Arrays on rGO/CNTs and Their Application in Electrochemical Capacitors, *Adv. Funct. Mater.*, 2012, **22**, 2560-2566; (c) K. K. Lee, W. S. Chin and C. H. Sow, Cobalt-Based Compounds and Composites as Electrode Materials for High-Performance Electrochemical Capacitors, *J. Mater. Chem. A*, 2014, **2**, 17212–17248.

6 (a) D. Cai, D. Wang, B. Liu, L. Wang, Y. Liu, H. Li, Y. Wang, Q. H. Li and T. H. Wang, Three-Dimensional Co_3O_4@$NiMoO_4$ Core/Shell Nanowire Arrays on Ni Foam for Electrochemical Energy Storage, *ACS App. Mater. Interfaces*, 2014, **6**, 5050–5055; (b) Z. Li, J. Han, L. Fan, M. Wang, S. Tao and R. Guo, The Anion Exchange Strategy towards Mesoporous α-$Ni(OH)_2$ Nanowires with Multinanocavities for High-performance Supercapacitors, *Chem. Commun.*, 2015, **51**, 3053–3056.

7 (a) C. Yuan, J. Li, L. Hou, X. Zhang, L. Shen, X.W. Lou, Ultrathin Mesoporous $NiCo_2O_4$ Nanosheets Supported on Ni Foam as Advanced Electrodes for Supercapacitors, *Adv. Funct. Mater.*, 2012, **22**, 4592–4597; (b) C. Z. Yuan, L. Yang, L. R. Hou, L. F. Shen, X. G. Zhang and X. W. Lou, Growth of ultrathin mesoporous Co_3O_4 nanosheet arrays on Ni foam for high-performance electrochemical capacitors, *Energy Environ. Sci.*, 2012, **5**, 7883–7887; (c) Q. Yang, Z. Lu, X. M. Sun and J. F. Liu, Ultrathin Co_3O_4 Nanosheet Arrays with High Aupercapacitive Performance, *Sci. Rep.*, 2013, **3**, 3537.

8 X. Ge, C. D. Gu, X. L. Wang and J. P. Tu, Correlation between Microstructure and Electrochemical Behavior of the Mesoporous Co_3O_4 Sheet and Its Ionothermal Synthesized Hydrotalcite-like α-$Co(OH)_2$ Precursor, *J. Phys. Chem. C*, 2014, **118**, 911−923.

9 M. J. Jing, Y. C. Yang, Y. R. Zhou, H. S. Hou, Q. Y. Chen and X. B. Ji, Alternating Voltage Induced Porous Co_3O_4 Sheets: an Exploration of Its Supercapacity Properties, *RSC Adv.*, 2015, **5**, 177–183.

10 S. K. Meher and G. R. Rao, Ultralayered Co_3O_4 for High-Performance Supercapacitor Applications, *J. Phys. Chem. C*, 2011, **115**, 15646–15654.

11 C. Feng, J. F. Zhang, Y. He, C. Zhong, W. B. Hu, L. Liu and Y. D. Deng, Sub-3 nm Co_3O_4 Nanofilms with Enhanced Supercapacitor Properties, *ACS Nano,* 2015, **9**, 1730–1739.

12 L. Y. Chen, Q. Zhang, H. Xu, X. H. Hou, L. Y. Xuan, Y. Q. Jiang and Y. Yuan, Amorphous 3D Nanoflake Array-Assembled Porous 2D Cobalt–Oxalate Coordination Polymer Thin Sheets with Excellent Pseudocapacitive Performance, *J. Mater. Chem. A*, 2015, **3**, 1847–1852.

13 X. L. Xu, Z. H. Chen, Y. Li, W. K. Chen and J. Q. Li, Bulk and Surface Properties of Spinel Co_3O_4 by Density Functional Calculations, *Surf. Sci.*, 2009, **603**, 653–658.

14 (a) G. Anandha Babu, G. Ravi and Y. Hayakawa, Microwave synthesis and effect of CTAB on ferromagnetic properties of NiO, Co_3O_4 and $NiCo_2O_4$ nanostructures, *Appl. Phys. A*, 2015, **119**, 219–232; (b) S. Balasubramanian and P. K. Kamaraj, Fabrication of Natural Polymer Assisted Mesoporous Co_3O_4/Carbon Composites for Supercapacitors, *Electrochim. Acta*, 2015, **168**, 50–58.

15 (a) C. Z. Yuan, L. H. Zhang, L. R. Hou, G. Pang and W. C. Oh, One-Step Hydrothermal Fabrication of Strongly Coupled Co_3O_4 Nanosheets–Reduced Graphene Oxide for Electrochemical Capacitors, *RSC Adv.*, 2014, **4**, 14408-14413; (b) F. L. Meng, Z. G. Fang, Z. X. Li, W. W. Xu, M. J. Wang, Y. P. Liu, J. Zhang, W. R. Wang, D. Y. Zhao and X. H. Guo, Porous Co_3O_4 Materials Prepared by Solid-State Thermolysis of a Novel Co-MOF Crystal and Their Superior Energy Storage Performances for Supercapacitors, *J. Mater. Chem. A*, 2013, **1**, 7235–7241.

16 M. Huang, X. Zhao, F. Li, W. Li, B. Zhang and Y. Zhang, *J. Mater. Chem. A*, Synthesis of Co_3O_4/SnO_2@MnO_2 Core–Shell Nanostructures for High-Performance Supercapacitors, 2015, **3**, 12852–12857.

17 H. B. Wu, H. Pang and X. W. Lou, Facile Synthesis of Mesoporous $Ni_{0.3}Co_{2.7}O_4$ Hierarchical Structures for High-Performance Supercapacitors, *Energy Environ. Sci.*, 2013, **6**, 3619–3626.

18 F. Hekmat, B. Sohrabi, M. S. Rahmanifar and M. R. Vaezi, Supercapacitive Properties of Coiled Carbon Nanotubes Directly Grown on Nickel Nanowires, *J. Mater. Chem. A*, 2014, **2**, 17446–17453.

19 H. H. Huo, Y. Q. Zhao and C. L. Xu, 3D Ni_3S_2 Nanosheet Arrays Supported on Ni Foam for High-Performance Supercapacitor and Non-Enzymatic Glucose Detection, *J. Mater. Chem. A*, 2014, **2**, 15111–15117.

20 Y. Zhang, Y. Liu, J. Chen, Q. Guo, T. Wang and H. Pang, Cobalt Vanadium Oxide Thin Nanoplates: Primary Electrochemical Capacitor Application, *Sci. Rep.*, 2014, **4**, 5687.

21 Y. Gogotsi, What Nano Can Do for Energy Storage, *ACS Nano*, 2014, **8**, 5369–5371.

22 S. Xiong, C. Yuan, M. Zhang, B. Xi and Y. T. Qian, Controllable Synthesis of Mesoporous Co3O4 Nanostructures with Tunable Morphology for Application in Supercapacitors, *Chem. Eur. J.*, 2009, **15**, 5320–5326.

23 L. Xie, K. Li, G. Sun, Z. Hu, C. Lv, J. Wang abd C. Zhang, Preparation and Electrochemical Performance of the Layered Cobalt Oxide (Co_3O_4) as Supercapacitor Electrode Material, *J. Solid State Electrochem.*, 2013, **17**, 55–61.

24 K. Deori, S. Ujjain, R. K. Sharma and S. Deka, Morphology Controlled Synthesis of Nanoporous Co_3O_4 Nanostructures and Their Charge Storage Characteristics in Supercapacitors, *ACS Appl. Mater. Interfaces*, 2013, 5, 10665−10672.

25 T. Zhu, J. S. Chen and X. W. Lou, Shape-Controlled Synthesis of Porous Co_3O_4 Nanostructures for Application in Supercapacitors, *J. Mater. Chem.*, 2010, **20**, 7015–7020.

26 D. L. Yan, H. Zhang, L. Chen, G. S. Zhu, S. C. Li, H. R. Xu and A. B. Yu, Biomorphic Synthesis of Mesoporous Co_3O_4 Microtubules and Their Pseudocapacitive Performance, *ACS Appl. Mater. Interfaces,* 2014, **6**, 15632−15637.

27 H. Pang, F. Gao, Q. Chen, R. M. Liu and Q. Y. Lu, Dendrite-like Co_3O_4 Nanostructure and Its Applications in Sensors, Supercapacitors and Catalysis, *Dalton Trans.*, 2012, **41**, 5862–5868.

28 J. P. Chen, X. Chen, J. S. Wu, F. Liu, X. B. Zhang and V. P. Dravid, Porous Cobalt Oxides with Tunable Hierarchical Morphologies for Supercapacitor Electrodes, *CrystEngComm*, 2012, **14**, 6702–6709.

29 Y. P. Wang, A. Q. Pan, Q. Y. Zhu, Z. W. Nie, Y. F. Zhang, Y. Tang, S. Q. Liang and G. Z. Cao, Facile Synthesis of Nanorod-Assembled Multi-Shelled Co_3O_4 Hollow Microspheres for High-Performance Supercapacitors, *J. Power Sources*, 2014, **272**, 107–112.

30 D. T. Dam and J. M. Lee, Three-Dimensional Cobalt Oxide Microstructures with Brush-like Morphology via Surfactant-Dependent Assembly, *ACS Appl. Mater. Interfaces,* 2014, **6**, 20729−20737.

31 M. X. Liao, Y. F. Liu, Z. H. Hu and Q. Yu, Novel Morphologic Co_3O_4 of Flower-like Hierarchical Microspheres as Electrode Material for Electrochemical Capacitors, *J. Alloys Compds.,* 2013, **562**, 106–110.

32 X. Wang, A. Sumboja, E. Khoo, C. Yan and P. S. Lee, Cryogel Synthesis of Hierarchical Interconnected Macro-/Mesoporous Co_3O_4 with Superb Electrochemical Energy Storage, *J. Phys. Chem. C,* 2012, **116**, 4930−4935.

33 Y. H. Xiao, S. J. Liu, F. Li, A. Q. Zhang, J. H. Zhao, S. M. Fang and D. Z. Jia, 3D Hierarchical Co_3O_4 Twin-Spheres with an Urchin-Like Structure: Large-Scale Synthesis, Multistep-Splitting Growth, and Electrochemical Pseudocapacitors, *Adv. Funct. Mater.,* 2012, **22**, 4052–4059.

34 F. L. Luo, J. Li, Y. Lei, W. Yang, H. Y. Yuan and D. Xiao, Three-Dimensional Enoki Mushroom-like Co_3O_4 Hierarchitectures Constructed by One-Dimension Nanowires for High-Performance Supercapacitors, *Electrochim. Acta,* 2014, **135**, 495–502.

35 Y. Y. Wang, Y. Lei, J. Li, L. Gu, H. Y. Yuan and D. Xiao, Synthesis of 3D-Nanonet Hollow Structured Co_3O_4 for High Capacity Supercapacitor, *ACS Appl. Mater. Interfaces,* 2014, **6**, 6739−6747.

36 Y. Fan, G. J. Shao, Z. P. Ma, G. L. Wang, H. B. Shao and S. Yan, Ultrathin Nanoflakes Assembled 3D Hierarchical Mesoporous Co_3O_4 Nanoparticles for High-Rate Pseudocapacitors, *Part. Part. Syst. Charact.,* 2014, **31**, 1079–1083.

37 Y. H. Xiao, A. Q. Zhang, S. J. Lu, J. H. Zhao, S. M. Fang, D. Z. Jia and F. Li, Free-Standing and Porous Hierarchical Nanoarchitectures Constructed With Cobalt Cobaltite Nanowalls for Supercapacitors with High Specific Capacitances, *J. Power Sources,* 2012, **219**, 140–146.

38 W. L. Yang, Z. Gao, J. Ma, J. Wang, B. Wang and L. H. Liu, Effects of Solvent on the Morphology of Nanostructured Co_3O_4 and Its Application for High-Performance Supercapacitors, *Electrochim. Acta,* 2013, **112**, 378–385.

39 Y. Z. Zhang, Y. Wang, Y. L. Xie, T. Cheng, W. Y. Lai, H. Pang and W. Huang, Porous Hollow Co_3O_4 with Rhombic Dodecahedral Structures for High-Performance Supercapacitors, *Nanoscale*, 2014, **6**, 14354–14359.

Graphic Abstract

Engineering 2D Multi-Layer Graphene-like Co_3O_4 Thin Sheets with Vertically Aligned Nanosheet as Basic Building Units for Advanced Pseudocapacitor Materials

Lingyun Chen*[a,b], Liying Xuan[a], Qingqing Yang[a], Xiaohuan Hou[a], Yuqian Jiang[a], Qing Zhang[a] and Yuan Yuan[a]

Abstract

Olivaceous 2D multi-layer graphene-like Co_3O_4 thin sheets (CQU-Chen-Co-O-1) with vertically aligned nanosheet as basic building units were first prepared on a large scale by direct hydrothermal decomposition of the mixed aqueous solution of cobalt (II) nitrate and acetic acid and exhibit excellent pseudocapacitive performances.